ASSESSMENT OF SENSOR CHARACTERISTICS OF AN AIRBORNE LASER SCANNER USING GEOMETRIC REFERENCE TARGETS

Lukas Wotruba[1], Felix Morsdorf[1],* Erich Meier[1], Daniel Nüesch[1]

1) Remote Sensing Laboratories
Department of Geography
University of Zurich

Working Group III/3

KEY WORDS: laser scanning, accuracy, high resolution, point clouds, sensor specifications

ABSTRACT

In order to get an experimental insight on the characteristics of a modern airborne laser scanning system, we carry out a set of experiments using geometrical targets on an air strip and use different flying heights. Sensor noise and relative accuracy is evaluated through 4 cardboard tables, being plain and homogeneously reflecting. The standard deviation of all laser returns from such a target decreases with lower flying altitude, as well as positional offsets computed tend to increase with flying altitude. The positional error along track is smaller than across track, probably due to different point spacing in these two directions. Target size and reflectance effects are assessed using wooden slats of different widths and colors. The effect of reflectance on target visibility is much larger than the effect of target size, which is in agreement to theoretical findings. Effective footprint size is attempted to be determined by slats with high reflectance forming a star. The difference between geometric (computed only by beam divergence) and effective footprint size increases with measurement distance, with the effective diameter being smaller than the geometric one.

1 INTRODUCTION

LIght **D**etection **A**nd **R**anging (LIDAR) is able to deliver coordinates on a reflecting surface based on an accurate measurement of position and orientation of a sensor platform and a time of flight measurement of a laser pulse. An introduction to airborne laser scanning was given by Wehr and Lohr [1999], while a comprehensive summary of it's underlying theory is given by Baltsavias [1999]. Airborne laser scanning first was only a tool for generating digital terrain models [Kraus and Pfeifer, 1998; Petzold et al., 1999], but soon its use was extended to more complex applications such as vegetation analyses [Hyyppae et al., 2001; Naesset, 2002; Lefsky et al., 2002] and building reconstruction [Haala and Brenner, 1999; Brenner, 2005]. Despite this broad field of applications, relatively little is known about the interaction of the laser pulse with its reflecting objects. This information will become increasingly important for applications that use the raw laser data instead of raster models (e.g. [Morsdorf et al., 2004; Roggero, 2001]). For generating raster models, in most cases several echos are combined for one raster pixel, thus reducing random errors in height and position. Systematic errors, e.g. introduced through reflectance effects, however will affect as well raster models. Most small footprint scanners rely on some sort of thresholding the return signal to trigger their first and last or even multiple returns. Many effects influence the triggering of an echo from the return signal, e.g. the object's geometrical properties and reflectance, the sensor characteristics (beam divergence, thresholding algorithm) and viewing geometry (incident angle and distance to object). For simple geometric objects such as houses and roads, these effects are quite easy to handle. The added noise (e.g. through reflectance changes) to single measurements will add some uncertainty to the position and orientation of the objects; but they remain 'visible' in the raw laser data due to their inherent geometry, provided this geometry is large enough to capture a significant amount of laser echos. For complex surfaces such as e.g. vegetation, the nature of the triggered returns is much less evident. For instance, it is known that tree height is systematically underestimated by laser scanners not only due to sampling effects, but also by penetrating the canopy until a critical vegetation density is reached to trigger e.g. a first return [Gaveau and Hill, 2003; Morsdorf et al., 2004]. If a vegetation density can be considered critical in this context depends on quite a few factors: distribution, size and reflectance of canopy elements, foot print size and laser beam energy distribution. Attempts have been made to use geometrical and statistical models of vegetation to model the return waveform of large footprint sensors [Sun and Ranson, 2000; Ni-Meister et al., 2001], but this has not been carried out for small footprint data. However, the same principles can be applied, just at much smaller scales. If, for large footprint sensors (diameter $\sim 10m$) tree size and distribution are important parameters, with small footprint scanners (diameter $\sim 1m$) we need to address canopy characteristics at the branch and leaf level. But for these modeling approaches, a detailed knowledge about the sensor characteristics is needed. Our objective is to use self constructed geometric reference targets to infer estimates of sensor characteristics in respect to effective footprint size, echo separation, reflectance effects as well the dependence of these effects on flying height.

2 LASER-SCAN DATA

The LIDAR system used was the Falcon II Sensor developed and maintained by the German company TopoSys. The specifications of the TopoSys Falcon II system can be taken from Table 1. The system is a fiber array laser altimeter recording both first and last reflection from the laser signal (first/last echo). For some return signals, only
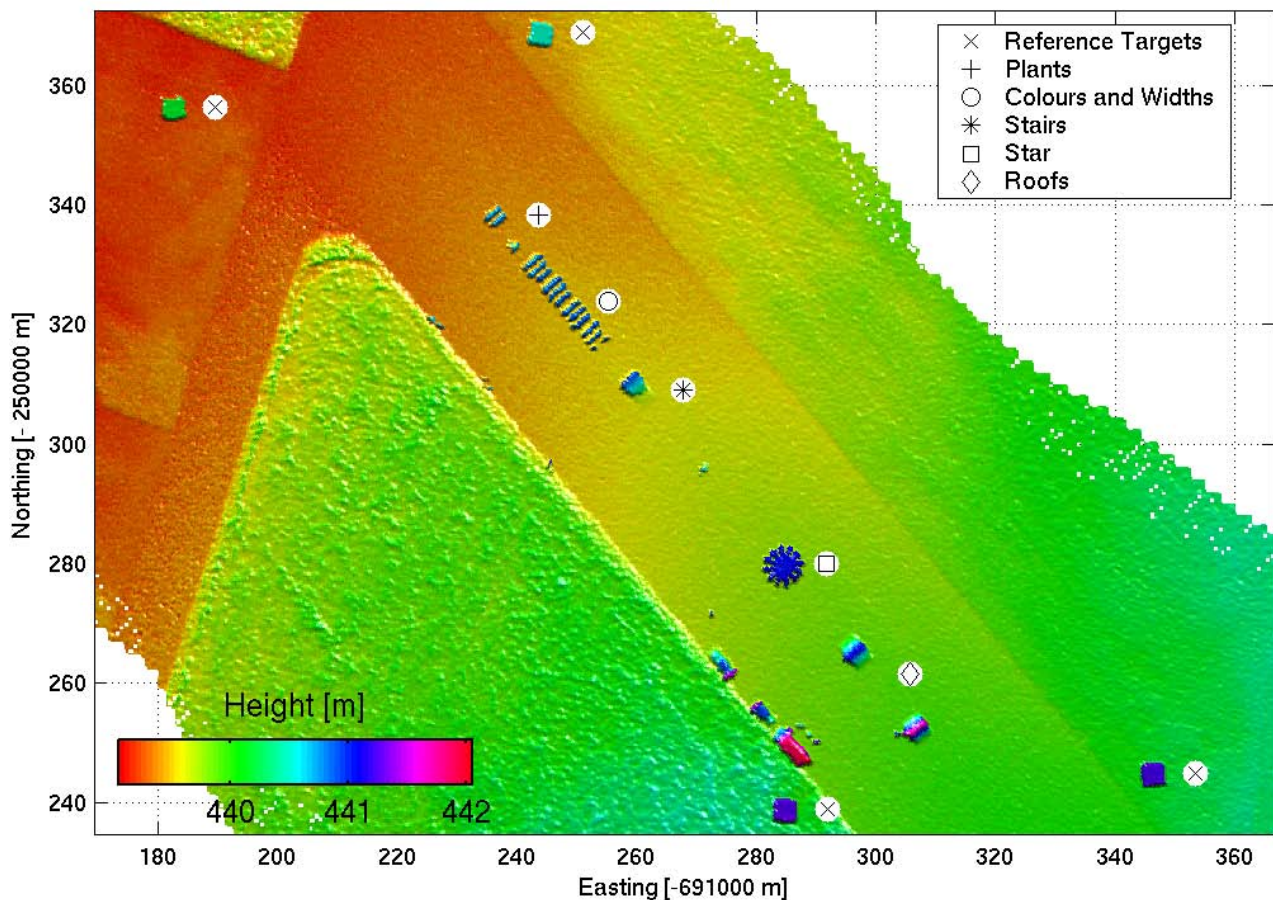
Figure 1: The Digital Surface Model (DSM) of our study site, an air strip. The positions of our reference targets are marked by white circles with the respective marker being explained in the legend. The DSM is from one of the 500 m above ground flights. The stair and the roof targets are not discussed in this paper due to the constraints in paper length.

one echo is triggered, meaning that both first and last echo have the same values in x,y,z, which we will call *single echo*. This is a special case for very dense or opaque targets.

Falcon II Specifications	
Maximum Range	1600 m
Range Resolution	2 cm
Scanning Angle	$\pm 7.15°$
Line-scan Frequency	653 Hz
Pulse Frequency	83 kHz
Laser Wavelength	1560 nm
Number of Fibers	127
Beam Divergence	1 mrad

Table 1: Specifications of Falcon II Sensor Platform

The raw data delivered by the sensor (x,y,z - triples) was processed into gridded elevation models by TopoSys using the company's processing software, TopPIT. The Digital Surface Model (DSM) was processed using the first echo reflections, the Digital Terrain Model (DTM) was constructed using the last returns and filtering algorithms.

3   EXPERIMENT SETUP

We set up a collection of geometric reference targets on an air-strip about 10 kilometers north-east of Zurich, Switzerland. For georeferencing, 4 cardboard covered tables were put up at the four corners of our experiment area being roughly 120 by 180 meters in size. These tables have first been used in Morsdorf et al. [2004], a more detailed description is given there. They were used to compute the planimetric offsets, height offset and height variations of the raw laser data. A detailed discussion of these values can be found in Section 3.1. Furthermore, a set of geometric reference target was constructed to gain insights in different sensor aspects. The test site was over flown in different heights, with four flights being 500 m AGL and one each for 700, 900 and 1100 m AGL. The flight direction was parallel to the air strip, and all geometric targets were setup along a line in the middle of the air strip, as can be seen in Fig. 1. We will only focus on three types of targets due to constraints in paper length, which will be presented in detail in the following sections.

3.1 Reference Targets

The quality of the LIDAR data was assessed using 4 geometric reference targets being 3 by 3 meter in size. The targets were leveled to less than 0.5 degrees, using a digital angle meter. The positions of the 4 corners of each target were determined using a GPS and theodolite measurements, resulting in an internal accuracy of less than 2 cm. Regarding the models (**DSM/DTM**), the absolute positional accuracy was determined by Toposys (using the target positions) to be similar to or less than the resolution of the models, with horizontal positional accuracy being better than 0.5 m and vertical accuracy better than 0.15 m.

3.2 Colors and Widths
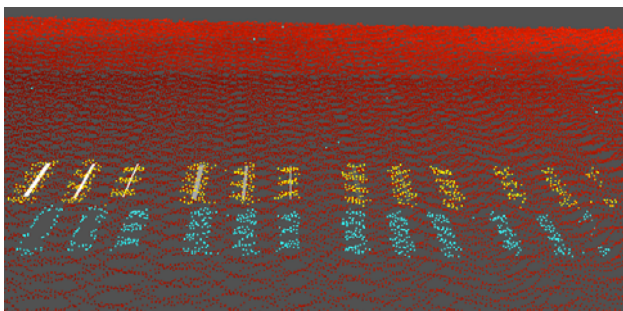
Figure 2: Slats with four different colors, white, light grey, dark grey and black (from left to right) and three different widths, 15, 10 and 5 cm (from left to right for each color). The length of the slats was three meter each. The lidar raw data from all 500 m AGL flights is superimposed. First echo data is colored orange to red, last echo data is colored cyan to magenta.

Wooden slats with three different widths and four different colors, each three meter long were set up about 1 meter apart. Their orientation was perpendicular to the flying direction, and the height over ground was 1.5 meters (see Fig. 2). The slat positions (as well as all other target positions) were measured using a theodolite. This target was intended to deliver some insights on the reflectance and width needed to trigger echos at different flying heights. The reflectance values of the different colored slats have been measured using an Advanced Spectral Devices (ASD) field spec and are listed in Table 2. All spectra were converted to absolute reflectance by reference measurements over a Spectralon panel with known spectral properties. Since the TopoSys system has a small scanning angle of $\pm7.15°$, the values for the nadir view should be representative.

3.3 Star

The star target (Fig. 3) was constructed to get an estimate of the effective footprint size. The fraction of area covered by the target versus the area covered by ground increases from outside to inside, thus simulating different densities.

Color	Reflectance at 1560 nm		
	Forward	Orthogonal	Nadir
Black	0.06	0.02	0.02
Dark Grey	0.14	0.09	0.1
Light Grey	0.42	0.12	0.16
White	0.66	0.48	0.52

Table 2: Reflectance values at laser beam wavelength for the different colored wooden slats. Three different views have been measured using an ASD field spec.
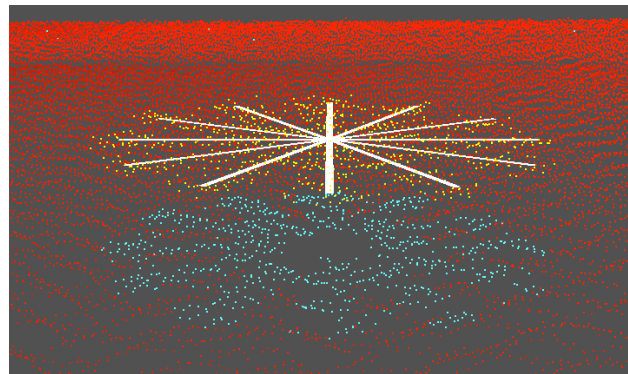
Figure 3: The *star* target. 12 white painted slats with a width of 5 cm were setup forming a star with a diameter of 6 meters and a height above ground of 1.5 m. The lidar raw data from all 500 m AGL flights is superimposed. First echo data is colored orange to red, last echo data is colored cyan to magenta.

4 RESULTS

4.1 Reference Targets

We used the reference targets to infer the noise of the sensor on a plain, homogeneously reflecting surface, which can be seen as a best case scenario. In order to get an estimate on the sensors noise, we calculated the standard deviation of all points reflected from the target. A slight flying height dependency of the noise can be derived from Table 3. The mean values for $\sigma height$ for 500 m AGL is 4.02 cm, while being 5.18 and 5.2 for 700 and 900 m AGL respectively. For 1100 m AGL, this value is again lower, being 4.63 cm. This could be explained through the lower amount of echos from the targets at 1100 m AGL. A positional offset was calculated by minimizing the distances from the raw laser data off the target to a simple square model in an iterative manner. The model of the square was shifted in it's x and y coordinates until a global minimum of distances was found. The values for offsets and noise are listed in Table 3. The offset have been calculated for along track and across track direction, with the presumption that errors might be systematically larger across track. This would be due to the different point spacing of the Falcon II system, with higher point spacing along track. The values in Table 3 for mean differences ($\overline{\Delta x}$ and $\overline{\Delta y}$) are a little larger for along track; for the standard deviations $(\Delta x)'$ and $(\Delta y)'$ the difference is larger, suggesting lower positional differences across track. Since we took a global flight angle for the separation of along track and across

AGL	$\overline{\Delta x}$ along track	$\overline{\Delta y}$ accr. track	$\Delta x'$ along track	$\Delta y'$ accr. track	$\overline{\sigma h}$	Pts.
$[m]$	$[m]$	$[m]$	$[m]$	$[m]$	$[cm]$	
1100	0.27	0.18	0.11	0.11	4.65	75
900	0.18	0.09	0.11	0.05	5.19	88
700	0.12	0.06	0.07	0.08	5.18	88
500	0.17	0.06	0.11	0.04	4.02	122

Table 3: Using the reference target data, we computed the mean positional offsets $\overline{\Delta x}$ and $\overline{\Delta y}$ for all four targets and their respective standard deviations $(\Delta x)'$ and $(\Delta y)'$, as well as the mean standard deviation of all laser points on a target $\overline{\sigma h}$ and its respective standard deviation $(\sigma h)'$ when combining the data from the four different targets. For 500 m AGL, all four flights have been used, making up for 16 single estimates of the respective values, as we have four reference targets. The last column gives the mean number of points on each target for each flying height.

track, some imprecise values may have been introduced in Table 3 due to rolling of the airplane, which can change the ratio of sampling densities locally. There should be as well a height dependency of positional accuracy, since the footprint size is increasing with flying height, and one has no means of determining *where* inside the illuminated spot the reflector was. For the positional offsets, this seem to be evident, with both mean and standard deviation being larger for 1100 and 900 m AGL than for 700 and 500 m AGL.

4.2 Colors and Widths

The target using different colors and widths was intended to yield an estimate at which width and reflectance first and/or last echo are triggered, under consideration of flying height. In Fig. 4 the results of these targets concerning first echos are depicted. Plotted is the relative visibility, that is the fraction of **first** echos on the target over ground returns, each for different widths (marked by symbols), different color (marked by color) and different flying heights (x-axis). For each of the slats, a section of the raw data with the slat width added to the expected diameter of the footprint (based on beam divergence) was cut out to do the statistics. One has to use caution with interpreting the data from 1100 m AGL, since only a few echos were contained in the raw data sections. As can be seen, at 500 and 700 m AGL and for the colors white, light grey and dark grey, a large amount of first echos (70-93 %) are on the target, there are only few first echos from the ground. It can be noted that the decrease of visibility with flying height is larger for the reflectivity than for slat size. Furthermore, the visibility seems to decrease in a more linear fashion for slat width (dashed lines) than for slat reflectivity, which exhibits some nonlinear behavior for the gray slats. The white and the black slats seem to lie above respective below a threshold of detection for all flying heights, except for 500 m AGL, where the black slats trigger almost 50 % first returns. The absolute numbers, however, have to be interpreted with caution, since for the higher flying height only few echos are available for the statistics. At 1100 m

AGL, only the white slats remain clearly visible, with more than 80 percent first echos on the target. The dark grey and black slats are only able to trigger less than 20 % first echos. However, as their nadir reflectance is very low (Table 2), it is surprising that there are *any* echos triggered by these slats. In Fig. 5 the first and last echo on the target are discriminated. The dark grey fill denotes the case of both first and last echo being the same *and* on the target. Light grey stands for first echo being different from last echo, with the first echo being on the target, while white stands for both single and first echo from the ground. Since the surface of the air strip was tarmac we only get single echos off the ground. The visibility of the targets decreases both with color and width, as well as with higher flying height. The wider slats (15 and 10 cm) and brighter slats (white and light grey) are able to trigger as well single echos at lower flying heights (500 and 700 m) as there is echo separation. This manifests a "shadowing" effect, which is also visible in Fig. 2 on the left. At 500 meter AGL, the wider ones of the white targets are able restrain echos (even last echos) from an area that is larger than slat width. This is a well known effect from for instance power lines, their LIDAR cross-section is often almost as large as almost double the footprint size. For higher flying heights (900 and 1100 m) there is no separation of footprints, a behavior that is visible as well for all other 'transparent' targets. One exception is the five centimeter wide black slat at 900 m AGL, which triggers one separated echo. This hints towards a possible explanation of the observed height dependence of echo separation. The reflectance difference seems to play a role if the vertical distance of two objects is close to the theoretical distance for echo separation, which is half the pulse length of the laser system. That is, two objects in that range may only be separable if their reflectance is similar, as is for the black slats and the tarmac.
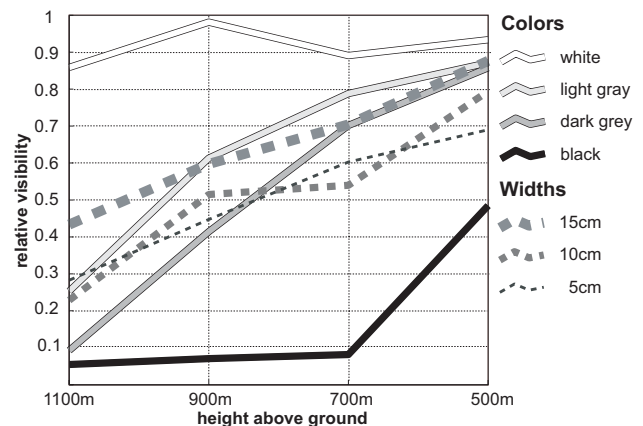
Figure 4: Height dependency of first returns statistics regarding the percentage of target hits in an area of slat width ± *geometric* footprint size. The legend gives information about the different colors and widths. For the widths, all 4 colors have been put together.

4.3 Star

According to Baltsavias [1999], one has to distinguish laser footprint diameter (geometric footprint diameter) and laser beam diameter, which is often defined by distance of two
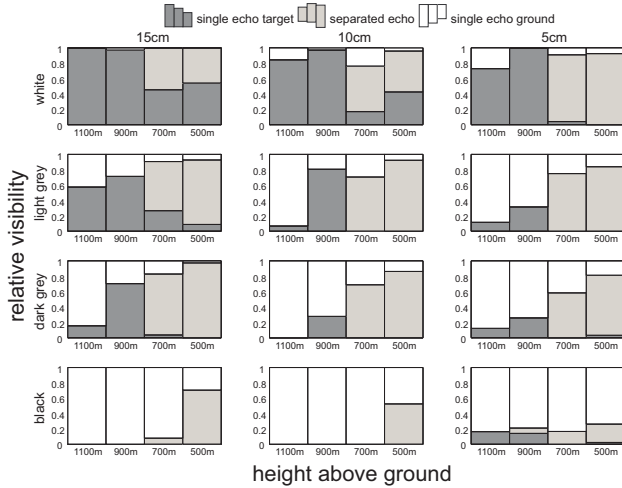
Figure 5: The percentage of target hits for the different colors (top to bottom) and different widths (left to right).The different colors denote different echo cases. White are ground echos (only single echos), light grey are separated echos (first always on target) and dark grey are single echos off the target. The different flying heights are labeled at the bottom of each plot.
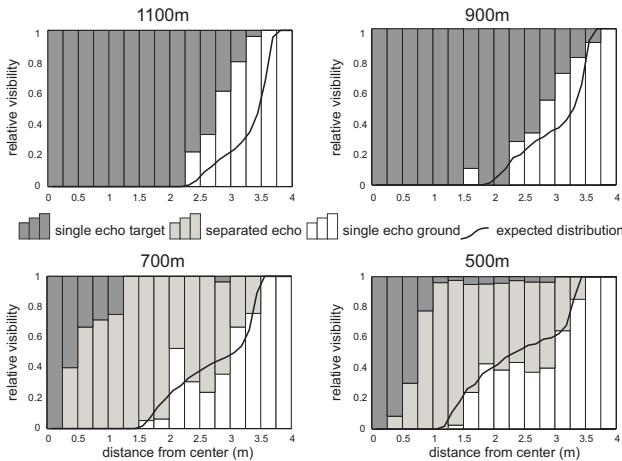
Figure 6: The ratio of echos from target to all echos from the center of the star to the outside. Color denotes the type of echo. The four panels are four different flying heights. For 500 m, all four flights have been put together.

opposing point in a beam cross section at a certain energy value, e.g. $1/e^2$ of the intensity at the beam center. We define another footprint size, the effective footprint, which will depend as well on the reflectivity of the target. Thus, it will give us an estimate on how large the footprint can be in order to fit in-between two slats without triggering a first echo. From Fig. 6 one can draw that there is no first and last echo separation for 1100 and 900 meter AGL. There are either single echos on the target or single echos on the ground, with a transition zone between the two cases, which starts at 2.5 m from the star center (1100 m AGL) or at about 2 m distance from the star's center point (900 m AGL). From the position of this transition zone, one can infer the size of the effective footprint, since at that distance the laser pulses fit in between the wooden

slats. Effective means that not only the simple geometric footprint size based on beam divergence is used, but that the energy distribution across the laser beam is accounted for as well. This effective footprint will depend on the targets reflectivity, for instance, if we would have build the star using aluminum foil, we would have measured larger effective footprint diameters. It should be noted that the values for effective footprint size are less reliable for the higher flying heights, since the sampling density was not high enough to ensure that every density (radius) of the star target was effectively hit by a laser pulse. From Fig 6 one can draw as well that the size of the effective footprint is height dependent. The black lines denote simulated percentages for hit target/hit ground based on the geometric laser footprint. The simulation was carried out adding a virtual buffer as large as the geometric footprint to the target. This new object is now being sampled with a large amount of infinitesimally small impulses, thus constructing a virtual data-set of laser echos containing only either target or ground hits. This data-set is treated in the same way as the real laser data to yield the percentages depicted as dashed line in Fig. 6. For the geometric footprint size, Baltsavias [1999] introduced following equation:

$$A = D + 2\,h\,tan(\frac{\gamma}{2}) \qquad (1)$$

A is the footprint diameter, D the diameter of the aperture of the laser scanner (which is 6 cm for the Falcon II system), h the flying height above ground and γ the beam divergence. For the geometric footprint size, Equation 1 can be used, but often the sensor aperture D is neglected. At 500 m AGL the effective footprint size seems to be larger than the geometric one calculated using Eq. 1. This can be concluded by the simulated curve being above the ground echo distribution, opposed to the other three flying altitudes. This suggests that D can not be neglected from Eq. 1 for low flying heights. Due to signal strength issues one will not notice this effect for higher flying heights or low reflecting targets, since there the effective footprint is always smaller than the geometric footprint.

5 DISCUSSION AND CONCLUSIONS

We have successfully conducted a set of experiments regarding sensor characteristics of an airborne laser scanning system. Most of our findings are in good agreement with theoretical concepts, but our work furthermore allows some insights on absolute numbers of sensor properties in a practical context. The noise contained in return echos from a plane, homogeneously reflecting surface seems to be height dependent, with lower noise at low flying altitudes. This could probably be caused by edge effects, as with larger flying heights a higher number of echos have their beam diameter not fully contained on the target. As expected from theory, point density and footprint size have an effect on positional accuracy, even though our data does not show a clear linear relationship. This could be due to sampling issues, since for higher flying heights, our targets are sampled by fewer echos. Based on the findings from Section 4.2 we can set up the following rule of thumbs:

- target size is less important than target reflectivity in respect to a targets visibility.

- the flying height dependence of target visibility due to reflectivity is stronger than for target size

- footprint separation depends on flying height, probably caused through illumination and reflectance differences

In our case, with the artificial targets we build and the reflection properties we have, the effect of reflectance seems to be larger than the effect of target size. This as well can be founded by theory. But even for targets with a quite high reflectance of 0.52, as the white slats have, not every illumination of the slat might result in an echo for higher flying heights such as 1100 m AGL.

We used a target formed as a star to simulate different target to ground area ratios and to get an insight on the effective footprint size. That is, at which distance of two high reflecting slats will the laser beam fit in-between without triggering a first echo. The effective footprint seemed to be larger than the geometric laser footprint at 500 m AGL. This is probably due to the sidelobes of the gaussian energy distribution across beam below $1/e^2$ of the energy maximum containing sufficient energy for triggering returns for high-reflecting targets at low flying heights. In order to get a better estimate on the energy distribution across the laser beam, one could construct star targets using differently colored slats, e.g. for a star target made out of aluminum foil, the effective footprint size should be close to the geometric one. The effect of diffraction could not be studied with our targets, but as stated by Baltsavias [1999], it would only add some few centimeters to the laser footprint size. As the applications using airborne laser scanner data are getting more and more sophisticated, an sufficient knowledge of potential error sources and their approximate sizes becomes vital. For instance, two objects having the same size, but with different reflectivity, could be measured different in size, with the object having the higher reflectivity being larger. Intensity data, that nowadays most laser scanners provide, could help identifying problematic spots in the laser data set. Using geometric reference targets such as we constructed can help getting a practical insight on the characteristics of a laser scanner and the reliability of its delivered data. Even an inter-comparison or calibration of different sensors over the same reference site would be possible.

6 ACKNOWLEDGMENTS

References

Baltsavias, E. P., 1999. Airborne laser scanning: basic relations and formulas. ISPRS Journal of Photogrammetry & Remote Sensing 54(2-3), pp. 199–214.

Brenner, C., 2005. Building reconstruction from images and laser scanning. International Journal of Applied Earth Observation and Geoinformation 6(3-4), pp. 187–198.

Gaveau, D. and Hill, R., 2003. Quantifying canopy height underestimation by laser pulse penetration in small-footprint airborne laser scanning data. Canadian Journal of Remote Sensing 29, pp. 650–657.

Haala, N. and Brenner, C., 1999. Extraction of buildings and trees in urban environments. ISPRS Journal of Photogrammetry & Remote Sensing 54(2-3), pp. 130–137.

Hyyppae, J., Kelle, O., Lehikoinen, M. and Inkinen, M., 2001. A segmentation-based method to retrieve stem volume estimates from 3-d tree height models produced by laser scanners. IEEE Transactions on Geoscience and Remote Sensing 39, pp. 969–975.

Kraus, K. and Pfeifer, N., 1998. Determination of terrain models in wooded areas with airborne laser scanner data. ISPRS Journal of Photogrammetry & Remote Sensing 53, pp. 193–203.

Lefsky, M. A., Cohen, W. B., Parker, G. G. and Harding, D. J., 2002. Lidar remote sensing for ecosystem studies. BioScience 52(1), pp. 19–30.

Morsdorf, F., Meier, E., Kötz, B., Itten, K. I., Dobbertin, M. and Allgöwer, B., 2004. Lidar-based geometric reconstruction of boreal type forest stands at single tree level for forest and wildland fire management. Remote Sensing of Environment 3(92), pp. 353–362.

Naesset, E., 2002. Predicting forest stand characteristics with airborne scanning laser using a practical two-stage procedure and field data. Remote Sensing of Environment 80(1), pp. 88–99.

Ni-Meister, W., Jupp, D. L. B. and Dubayah, R., 2001. Modeling lidar waveforms in heterogeneous and discrete canopies. IEEE Transactions on Geoscience and Remote Sensing 39(9), pp. 1943–1958.

Petzold, B., Reiss, P. and Stüssel, W., 1999. Laser scanning - surveying and mapping agencies are using a new technique for the derivation of digital terrain models. ISPRS Journal of Photogrammetry & Remote Sensing 54(2-3), pp. 95–104.

Roggero, M., 2001. Airborne laser scanning: Clustering in raw data. International Archives of Photogrammetry and Remote Sensing XXXIV-3/W4, pp. 227–232.

Sun, G. and Ranson, K., 2000. Modeling lidar returns from forest canopies. IEEE Transactions on Geoscience and Remote Sensing 38(6), pp. 2617–2626.

Wehr, A. and Lohr, U., 1999. Airborne laser scanning - an introduction and overview. ISPRS Journal of Photogrammetry & Remote Sensing 54(2-3), pp. 68–82.